Natural Resources Canada | Ressources naturelles Canada

GEOMATICS CANADA
OPEN FILE 31

Mapping water bodies using SAR imagery – an application over the Spiritwood valley aquifer, Manitoba

J. Li and S. Wang

2017

Canada

GEOMATICS CANADA
OPEN FILE 31

Mapping water bodies using SAR imagery – an application over the Spiritwood valley aquifer, Manitoba

J. Li and S. Wang

2017

doi:10.4095/300213

This publication is available for free download through GEOSCAN (http://geoscan.nrcan.gc.ca/).

Recommended citation
Li, J. and Wang, S., 2017. Mapping water bodies using SAR imagery – an application over the Spiritwood valley aquifer, Manitoba; Geomatics Canada, Open File 31, 13 p. doi:10.4095/300213

Publications in this series have not been edited; they are released as submitted by the author.

Abstract

Canada has over 2 million lakes covering a total area of 0.9 million km^2. The inland water bodies play a critical role in water cycles, water resources, social economic including fisheries and recreation. However these inland aquatic ecosystems are under increasing pressure and big changes from increasing human activities and changing climate. To better understand the aquatic ecosystem dynamics and effectively manage the inland water bodies, it is essential to have up-to-date information of their spatial and temporal variability. Synthetic Aperture Radar (SAR), unlike optical sensors, is able to penetrate cloud, haze and smoke, and hence observe the earth's surface in all weather conditions day and night. SAR imagery is an effective method for mapping water bodies. This open file details the algorithms and their implementations for a novel method for mapping water bodies using SAR imageries. This method is completely automatic and less computational intensive, thus suitable for large scale applications. A test of this method over the Spritiwood valley in Manitoba using Radarsat-2/SAR data shows a high accuracy in delineating water bodies. This study provides a tool for mapping national scale inland water bodies and monitoring their dynamic changes in a near-real time environment.

1. Introduction

Almost 9%, or 0.9 million km^2, of Canada's total landmass is covered by fresh water in the form of lakes, rivers, and streams etc. The inland water bodies play an important role in the water cycles and surface water budget (Wang et al., 2014a; 2014b; 2014c) which strongly affect the atmosphere and surface/subsurface processes such as cloud development (Molders and Raabe, 1996), surface albedo (Wang et al., 2006), evapotranspiration (Wang et al., 2013), stream flow (Koster and Milly, 1997), and groundwater recharge (Sophocleous, 2002). Surface waters are also integral parts of groundwater flow systems and hence are indicators of the status of the overall fresh water resource. Increasing human activities and changing climate are increasing pressure and bringing big changes to these inland aquatic ecosystems. (Riordan et al., 2006; Smith et al., 2005; Yoshikawa and Hinzman, 2003). To effectively conserve and manage the fresh surface water resources, it is essential to have up-to-date information of their spatial and temporal variability. Satellite remote sensing is the only practical approach that can map surface water cost-effectively and in a timely manner (Rundquist et al. 2001).

Various optical satellite sensors such as Advanced Very High Resolution Radiometer (AVHRR), Moderate-resolution Imaging Spectroradiometer (MODIS), Landsat's MSS, TM/ETM+ and SPOT's HRV have been employed for surface water body detection (Campos et al., 2012; Du et al., 2012; Giardino et al, 2010; Huang et al, 2012; Jain et al, 2006; Ma et al., 2007; Sheng et al., 2001; Tulbure and Broich, 2013). The multispectral nature of optical sensors provides some advantages for water detection, however, their applications in detecting surface water are constrained by several environmental factors, such as cloudy sky condition, cloud shadows, smoke from wildfires and haze, etc (Brisco et al., 2009). SAR sensors have the ability to provide data for surface water body detection that can overcome the limitations of optical sensors. SAR imagery is an effective method for mapping water bodies (Brisco et al., 2009), and has been used for flood detection (Giustarini et al., 2013; Kuenzer et al., 2013; Lu et al., 2014; Martinis et al., 2009), monitoring open water dynamics (Bartsch et al., 2012), and delineating shorelines (Shu et al., 2010). Smooth water surfaces usually provide a specular reflection of microwave radiation, and hence very little energy is scattered back. In contrast, land surfaces scatter much more energy back to the radar due to, e.g., surface roughness and volume scattering. The difference in the energy received back leads to a high contrast between water and land.

Among the various supervised/unsupervised classification methods, histogram thresholding is one of the most popular approaches to delineate water bodies from land in SAR intensity imagery (Brisco et al., 2009; Brivio et al., 2002; Martinis, 2010). Li and Wang (2014) proposed an automatic method for mapping water bodies using SAR imagery. The method is based on histogram thresholding of the SAR texture image, which is not significantly influenced by the incidence angle. This work report details the algorithms and implementations of the method and its application over the Spritiwood valley in Manitoba. The report first describes the study area and datasets, followed by the details on the automatic method's algorithms and implementations. The application results are then analyzed and discussed. Summary of this study is presented in the last section.

2. Study area and datasets

The study area covers the Spiritwood buried valley (red polygon in figure 1) which extends from southwest Manitoba to North Dakota. The dominant land cover class is agriculture crops, intermingled with grassland, surface water bodies and forests. Surface water is fairly abundant in this area, in numerous small water bodies of the prairie landscape.

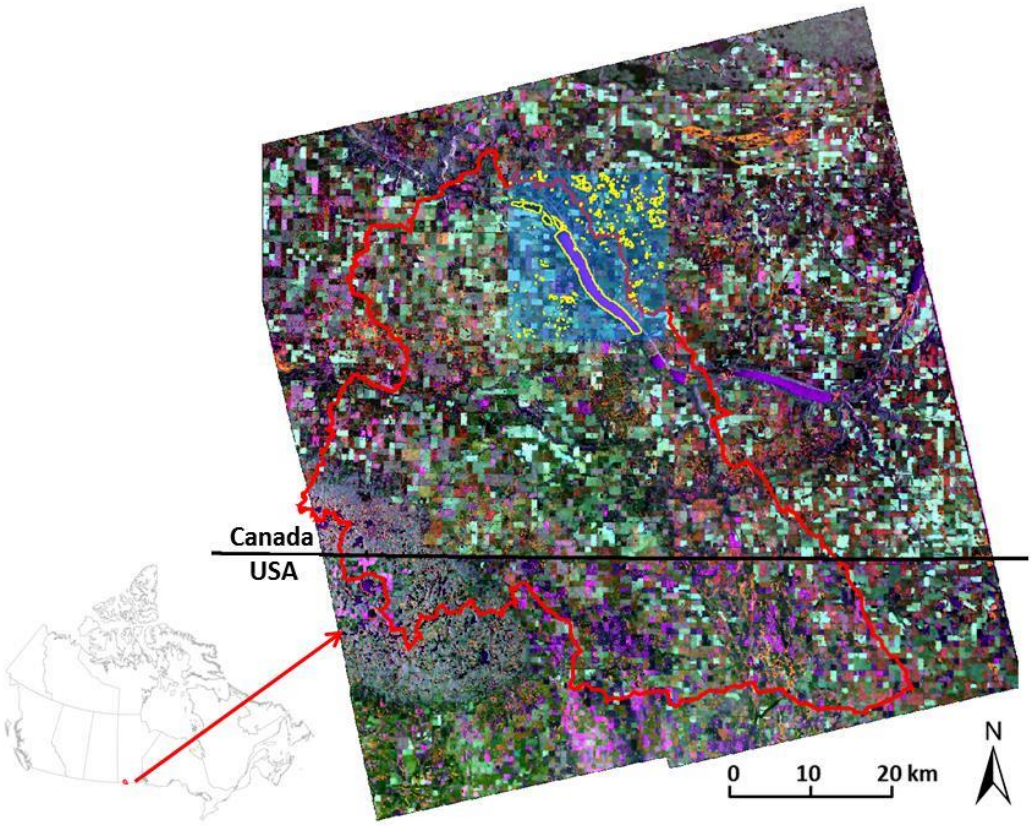

Figure 1. The location of study area (the red polygon show the boundary of the Spritiwood watershed) and ground truth reference map (highlighted in blue color) with water bodies (shown in yellow polygons) derived from 5m SPOT-5 image.

Radarsat-2 QuadPol (fully polarimetric mode) wide fine beam mode images (with a swath of 50 km and an azimuth resolution of 7.6 m) are used in the analysis. To cover the entire study area, two neighbor paths (4 scenes each path) were acquired on July 26, 2013 (FQ1W with incidence angle ~20°) and August 2, 2013 (FQ3W with incidence angle ~21.5°) and processed into a single-look

complex product type. All eight scenes of the image are first processed to generate calibrated multi-looking backscatter images, and then auto-orthorectified using the GAMMA program. The eight orthorectified images are mosaicked (with radiometric normalization) to one image with a resolution of 30 m. A 5 x 5 Enhanced Lee filter is applied to the mosaic image for speckle noise reduction. The mosaicking and filtering processes were completed in the PCI Geomatics. The background image in Figure 1 shows the composite of the HH (red), HV (green), and VV (blue) polarized images.

To assess the performance of the method, a reference map was created for a small portion of the Radarsat-2 mosaic image from the 5-m resolution SPOT-5 pan-sharpened multi-spectral image by visual interpretation and manual digitizing by using the ArcGIS software. The highlighted blue square in figure 1 indicates the location and coverage of the reference map. The reference map has 10% surface water shown in yellow and 90% land.

3. Method

The automated thresholding method presented in this report is based on the Otsu algorithm, which is one of the best threshold selection methods for image binarization (Fan and Lei, 2012). This method uses texture images to enhance the contrast between water and land in intensity images and use a modified Otsu thresholding algorithm to determine the optimal threshold value. The method is completely unsupervised (Li and Wang, 2014). An overview of the automated thresholding method for surface water detection in a SAR image is shown in Figure 2. The algorithms and implementations of this method are presented below:

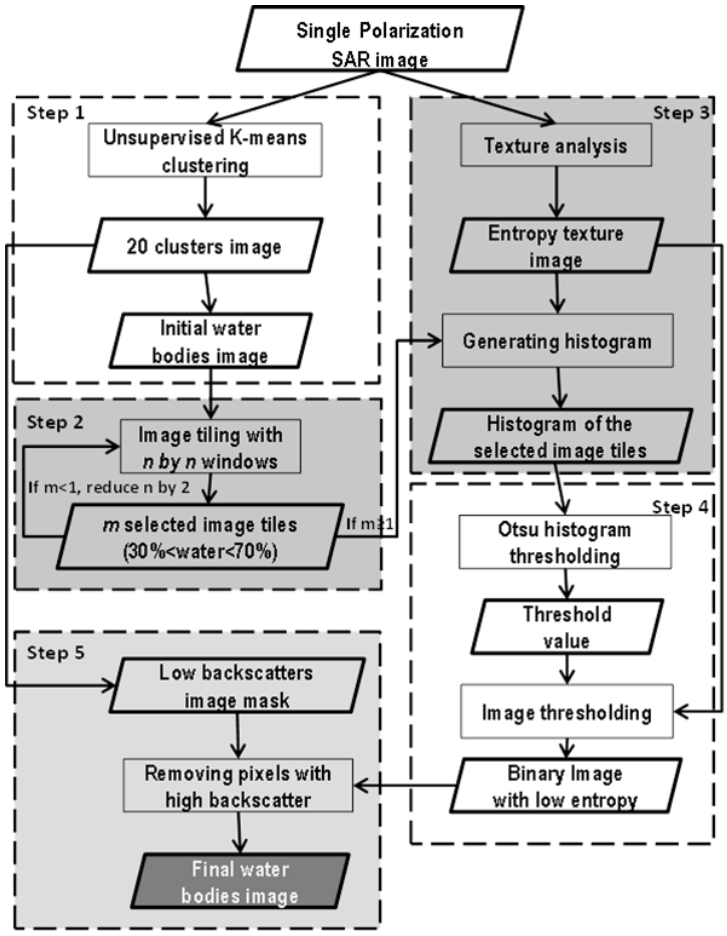

Figure 2. The flowchart of the method for water bodies detection.

Step 1: K-means cluster analysis. An initial water body mask, as well as a low backscatter image mask, is created by applying K-means clustering to the SAR intensity image. In general, this algorithm first randomly assigns K initial cluster centroids. The second step is to assign each pixel to its closest cluster centroid using Euclidian distance. In the third step, the new cluster centroids are calculated based on all the pixels in one cluster. The second and third steps are repeated until the cluster centroids don't change any more. The K-means algorithm provides fast execution and does not require a training stage to produce cluster centers. It can be easily implemented, however it has been implemented as a standard function in many remote sensing softwares. In this study, the SAR intensity image is first imported to the PCI Geomatic program, thus then the K-means

algorithm is applied to the SAR intensity image to obtain a map with initial *15* clusters. The cluster map encodes each cluster with a unique gray-level value. The cluster number is represented by the gray level. For example, cluster 1 is assigned a gray-level value of 1 corresponding to dark appearance in the SAR intensity image, and cluster 2 is assigned a gray-level value of 2, which may mix water and land. Using the EASI module in the PCI Geomatic program, We can easily generate the initial water body mask by assigning cluster 1 as water and other clusters as land, in which the water class may include some land pixels, as well as a low backscatter image mask, which is obtained by regrouping clusters 1 to 7 as low backscatter, and others as high backscatter.

Step 2: Sub-image selection. This step selects sub-images containing a sufficient proportion of land and water classes. To complete the sub-image selection, a SAR image *S* is divided into *M* non-overlapping sub-images with an analyst-defined size *w*w*. The selection of *w*, which determines *M*, depends on the extent of the two classes of water and land within the SAR image (Martinis et al, 2009). Due to the fact that Ostu algorithm is optimal for thresholding a histogram with a bimodal distribution, only sub-images, which contain a sufficient number of pixels from both water and land classes, are selected for the threshold computation. According to Bazi et al. (2007), it is sufficient for accurately detecting threshold values if each class has at least 10% of the pixels in an image. The criterion for water proportion in the sub-image selection is set to 10-90%. If no sub-image meets this criterion, the image partitioning process is repeated by decreasing *w* by 10 until sub-images with adequate water content are successfully extracted. A C++ program for this process was implemented with the initial water body mask image and the *w* as inputs. The output will be a mask image, named as sub-image mask, in which pixels of the selected sub-images are set to 1 and others are set to 0. The sub-image mask is the same size as the initial water body mask image.

Step 3: Entropy texture image histogram analysis. Texture is defined as tonal variation within a neighbourhood and thus reflects the spatial relations between pixels in an image. The texture information derived from a SAR image is a valuable feature for discriminating different land-cover types, and thus texture analysis has been widely used for image segmentation and land cover classification. Some studies have indicated that texture information is more useful than the intensity image for SAR image classification and segmentation (Song et al., 2007). Among the commonly used texture measures (e.g. variance, entropy, contrast et al.) computed from grey-level co-occurrence (GLCM), the entropy texture is often used in SAR image segmentation (Kekre et al., 2010; Samantal et al., 2011; Samanta and Sanyal, 2012). In this study, the surface water auto-detection strategy uses the entropy texture derived from the GLCM of SAR imagery. This step generates the entropy texture of the SAR intensity image in the PCI Geomatic program. The sub-image mask is then applied to extract entropy texture values of the sub-images and the histogram of the extracted entropy texture values is computed in a C++ program. The histogram computed in this program has to be normalized to a certain gray-level L (e.g. 255) for the Otsu algorithm. In this case the entropy texture image is also transformed to contain values from 0 ~ L (e.g. 255). This program accepts the sub-images mask, the entropy texture image and an analyst-defined gray-level L as inputs. The output includes the normalized histogram and the normalized entropy texture image.

Step 4: Otsu algorithm for automatically determining the threshold value. The Otsu algorithm is an automatic threshold selection method for the reduction of a grey-scale image to a binary image, which containing two classes. It selects an optimal threshold value separating those two classes so that the between-class variance is maximized. The advantage of this algorithm is that

only the grey-level histogram is needed to derive an image threshold without any other *a-priori* knowledge. The Otsu algorithm works well when the image histogram is close to a bimodal distribution with equal variances (Fan and Lei, 2012). In this study, although the sub-image selection process is employed to choose sub-images with bimodal distribution, the two classes may not have equal variances, which may result in an incorrect threshold value when applying the Otsu method. To improve the threshold selections in these cases, we use a modified Otsu method named valley-emphasis method proposed by Ng (2006). The valley-emphasis method makes the threshold closer to the actual valley of the histogram. It selects a threshold value that has small probability of occurrence (valley in the gray-level histogram), and also maximizes the between-class variance (Ng, 2006). Details for the modified Otsu method have been described by Li and Wang (2014). We implemented the modified Otsu algorithm in a C++ program. The program accepts the normalized histogram and the normalized entropy texture image obtained in Step 3 as inputs. An optimal threshold for the normalized histogram is computed and then applied to the normalized entropy texture image. The output is a mask image with low entropy.

Step 5: Generation of the final water body image. A low entropy mask image is obtained by applying the selected threshold to the normalized entropy texture image. The low backscatter image mask created in step 1 is used to refine the low entropy mask image to obtain the final water body image.

4. Results

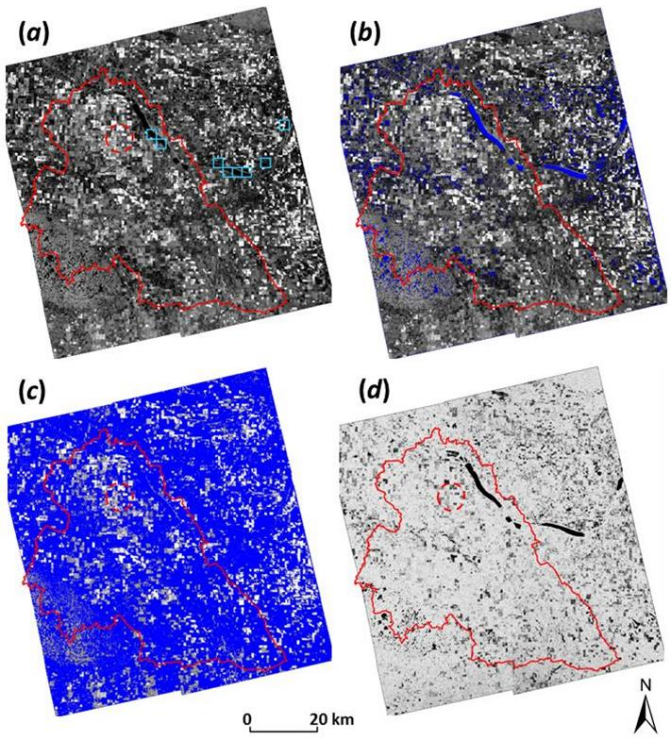

Figure 3. (a)The HV polarization intensity image; (b) the initial water bodies mask in blue color; (c) the low intensity mask in blue color; and (d) the entropy image derived from the HV intensity image.

The automatic histogram thresholding method (named as 'texture-method') was applied to the Radarsat-2 mosiac image over the Spritiwood valley in Manitoba. The HV polarization for the Radarsat-2 QuadPol mosaic data was chosen as the input to the method due to less effect of winds on this polarization. For the purpose of the performance assessment, we also test a 'traditional' method (denoted as 'intensity-method'), in which the valley enhanced Otsu algorithm is directly applied to the image intensity rather than the entropy texture after step 2 in the texture-method. The results obtained from both methods are then compared against the water polygons extracted from the 5 meter resolution SPOT-5 pan-sharpened multi-spectral image.

The initial water body mask and the low backscatter mask are generated by applying the K-means algorithm to the QuadPol SAR HV image. Figures 3(*a*), 3(*b*) and 3(*c*) show

the HV polarization intensity image, initial water body mask, and the low backscatter mask, respectively. It is found that the areal extent of initial water bodies occupy ~85% of the total water bodies by assigning the cluster 1 to water class. In the second step, the window size for image splitting is set to 100. A total of eight sub-images with size of 100 by 100 are selected. The cyan squares shown in Figure 3(*a*) indicate the location and coverage of these selected sub-images. Figures 3(*d*) shows the entropy texture image derived from the QuadPol SAR HV intensity image. The water bodies present low entropy and most of land areas show high entropy in the entropy texture image. Figures 3(*a*) and 3(*d*) indicate that the contrast between water and land in the entropy texture image increases substantially compared to that in the intensity image. One may notice that a few wetland (marsh) areas (e.g. the area highlighted by red circle), like water bodies, also present low entropy. However these areas show bright tone in the intensity image since their main scattering mechanism is the double bounce return of the standing water and grass. Therefore these wetland areas can be excluded in the histogram computation of sub-images by using the low backscatter mask image. Figure 4 shows the histograms of the selected sub-images: (*a*) the QuadPol HV intensity image and (*b*) the QuadPol HV entropy image. The histograms have been normalized to 256 grey levels. The intensity and entropy texture images are then transformed to contain values 0 ~ 255. The threshold values, 50 for the HV intensity image and 105 for the entropy image, are determined by the valley enhanced Otsu algorithm. The dash arrows in the figure 5 indicate the threshold positions (50 for the intensity-method, 105 for the texture-method) in the normalized histograms. The water body maps are generated by setting pixels with grey levels less than the determined threshold values as water. Some wetlands are, however, misclassified as water due to their low entropy values when the texture-method is used. The water body map is further refined by using the low backscatter mask which will eliminate those wetlands that present high backscatter and show bright tone in the intensity image.

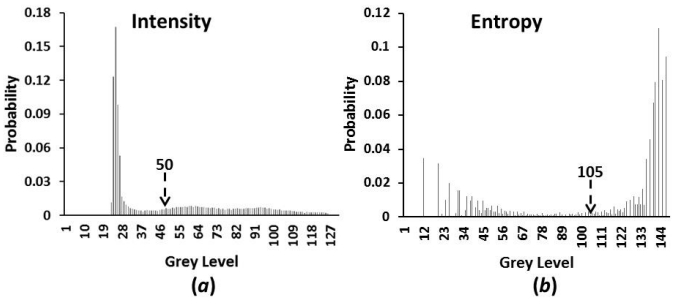

Figure 4. The histograms of the selected sub-images of (a) normalized HV intensity image and (b) normalized HV entropy image.

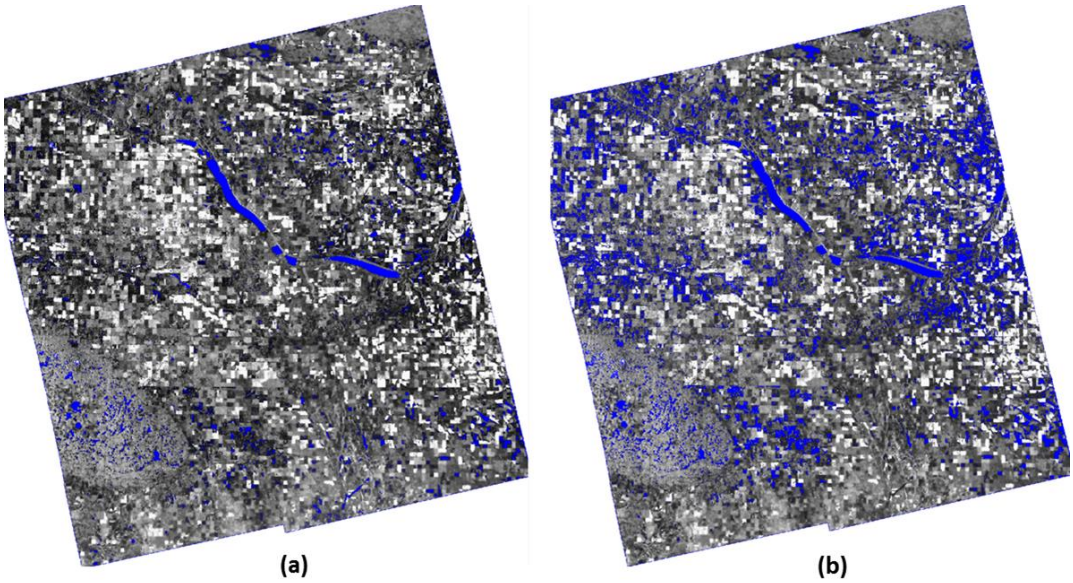

Figure 5. The surface water bodies (in blue color) detected by (a) the texture-method and (b) the intensity-method.

Figure 5 shows the final water body maps generated by the two methods: (a) the texture-method and (b) the intensity-method. One can notice that the intensity-method produces more surface water areas than the texture-method. Error matrices are generated to assess the performances of the two methods using around 8000 samples selected from the reference water body map derived from the 5m resolution SPOT-5 image.

Table 1. Error matrices of classification results from (a) texture-method and (b) intensity-method

(a) Texture-method

	Reference data		
Classified data	**Land**	**Water**	**Total**
Land	5314	263	5577
Water	146	2423	2569
Total	5460	2686	8146
Kappa index:		**0.89**	

(b) Intensity-method

	Reference data		
Classified data	**Land**	**Water**	**Total**
Land	5037	329	5366
Water	423	2357	2780
Total	5460	2686	8146
Kappa index:		**0.79**	

Table 1 shows the error matrices for the classification results from (a) the texture-method and (b) the intensity-method. From the error matrices, the Kappa indices can be calculated for evaluating the accuracy of water-land classifications. The Kappa indices indicate the texture-method (Kappa index = 0.89) has a higher accuracy than the intensity-method (Kappa index = 0.79) for the water-land classifications. For comparison, of 423 land pixels misclassified as water pixels in the intensity-method, the texture-method reduces the land-water mis-classification error to 146 pixels. This misclassification is attributable to the miscalculation of the threshold value in the intensity method. From the histogram in Figure 5(a), we notice that the land class in the intensity image presents a flat histogram with a long tail on the right side, which may result in a larger threshold value when the modified Otsu algorithm is used. Of total 2686 water reference pixels, the texture-method produces

409 (15.2%) error pixels (water misclassified as land and vice versa), in comparison to the 752 (28.0%) error pixels of the intensity method.

The texture-method has smaller classification error for the water pixels than the intensity-method. However, about 10% of the error for water pixels that are misclassified to land pixels is still measured. It might be explained by the different acquisition dates of the SPOT-5 and Radarsat-2 data and temporal changes in water level. Another error source may come from the edge pixels of water and land. Due to the 3 by 3 window operation in the computation process of the entropy texture, the edge pixels of a water body may have higher entropy than the inside pixels, which may result in misclassifying water as land. Therefore the classification accuracy could be improved by expanding one pixel of the detected water bodies, which needs to be verified with the applications of a morphological operator in future studies. Table 1 indicates that about 3% of the land pixels are misclassified as water. A probable reason for this is the confusion of water and roads. Roads present the same backscattering mechanic as water, and consequently roads also appear as a dark color in a SAR image. This error could be further reduced by using the existing road network data.

5. Summary

This report details the algorithms and implementations of the automatic texture thresholding method for mapping water bodies using SAR imagery. Application to a Radasat-2 mosaic scene over the Spritiwood valley in Manitoba demonstrated a satisfactory result (Kappa index = 0.89). The method combines the K-means clustering algorithm, sub-image selection process, and a modified Otsu thresholding algorithm. Using K-means clustering, the sub-images, which contain sufficient proportions of water and land classes, are selected. It is critical for the Otsu algorithm to detect an optimal threshold for a SAR image. Compared to the intensity image, the entropy texture image can enhance the contrast between water and land and reduce the variability in grey level for the land class. An improved result is obtained when the Otsu algorithm is applied to the entropy texture image. The results show higher classification accuracy and lower classification error than the commonly used intensity-method for overall land-water classification. The results also indicate that the water bodies in a large SAR image can be delineated from land automatically by the texture-method. The method can be applied to a single geocoded SAR image, with no additional data (other than DEM data for geo-orthrectification) required. This texture-method is completely automatic and less computational intensive, thus suitable for large scale applications. All algorithms used in the texture-method provide fast execution. These advantages mean that it can be easily implemented and could be a tool for mapping national scale water bodies and monitoring their dynamic changes in near-real time. The algorithms of this method have been implemented by using C++ programming language.

Acknowledgements

This work was supported by the Groundwater Geoscience Program and the Remote Sensing Science Program of the Earth Science Sector (ESS), Natural Resources Canada. We gratefully thank Dr. Hazen Russell of the Geological Survey of Canada for managerial support.

References:

Bartsch, A., A. M. Trofaier, G. Hayman, D. Sabel, S. Schlaffer, D.B. Clark, and E. Blyth. 2012. "Detection of open water dynamics with ENVISAT ASAR in support of land surface modelling at high latitudes." *Biogeosciences* 9 (2): 703-714.

Bazi, Y., L. Bruzzone, and F. Melgani. 2007. "Image thresholding based on the EM alg-orithm and the generalized Gaussian distribution." *Pattern Recognition* 40(2): 619–634.

Brisco, B., N. Short, J. J. van der Sanden, R. Landry, and D. Raymond. 2009. "A semi-automated tool for surface water mapping with Radarsat-1." *Canadian Journal of Remote Sensing* 35**(**4): 336-344.

Brivio, P.A., R. Colombo, M. Maggi, and R. Tomasoni. 2002. "Integration of remote sensing data and GIS for accurate mapping of flooded areas." *International Journal of Remote Sensing* 23(3): 429–441.

Campos, J.C., N. Sillero, and J.C.Brito. 2012. "Normalized difference water indexes have dissimilar performances in detecting seasonal and permanent water in the Sahara-Sahel transition zone." *Journal of Hydrol*ogy *464-465*: 438–446

Drake, B. and K. Patton. 1980. "Land use/cover mapping from SEASAT-A radar of the greater part of the Delmarva Peninsula, USA." Proceedings of the 14th International Symposium on Remote Sensing of Environment, Environmental Research Institute of Michigan, Ann Arbor, USA, 1565–1575.

Du, Z., B. Linghu F. Ling, W. Li, W. Tian, H. Wang, Y. Gui, B. Sun and X. Zhang. 2012. "Estimating surface water area changes using time-series Landsat data in the Qingjiang River Basin, China." *Journal of Applied Remote Sensing 6(1)*, 063609 (Nov. 28, 2012). http://dx.doi.org/10.1117/1.JRS.6.063609.

Fan, J. L., and B. Lei. 2011. "A modified valley-emphasis method for automatic thresholding. 2011." *Pattern Recognition Letter* 33(6): 703-708.

Giardino, C., M. Bresciani, P. Villa, and A. Martinelli. 2010. "Application of remote sensing in water resource management: the case study of Lake Trasimeno, Italy." *Water Resource Manage*ment *24(14)*: 3885–3899.

Giustarini, L., R. Hostache, P. Matgen, G. J. P. Schumann, P. D. Bates, and D. C. Mason. 2013. "A change detection approach to flood mapping in Urban areas using TerraSAR-X." *IEEE Transactions on Geoscience and Remote Sensing* 51(4): 2417-2430.

Huang, S., J. Li, and M. Xu. 2012. "Water surface variations monitoring and flood hazard analysis in Dongting Lake area using long-term Terra/MODIS data time series." *Natural Hazards 62(1)*: 93–100.

Jain, S.K., A.K. Saraf, A.Goswami and T. Ahmad. 2006. "Flood inundation mapping using NOAA AVHRR data." *Water Resource Management 20(6)*: 949–959.

Kekre, H. B. and S. Gharge. 2010. "Texture based segmentation using statistical properties for mammographic images." *International Journal of Advanced Computer Science and Applications* 1(5): 102-107.

Koster, R. D. and P. C. D. Milly. 1997. "The Interplay between Transpiration and Runoff Formulations in Land Surface Schemes Used with Atmospheric Models." *Journal of Climate* 10(7): 1578-1591.

Kuenzer, C., H. Guo, I. Schlegel, V.Q. Tuan, X. Li, and S. Dech, S. 2013. "Varying scale and capability of Envisat ASAR-WSM, TerraSAR-X Scansar and TerraSAR-X Stripmap data to assess urban flood situations: A case study of the Mekong delta in Can Tho province." *Remote Sensing* 5(10): 5122-5142.

Li, J. and S. Wang. 2014. "An automatic method for mapping inland surface water bodies with Radarsat-2 imagery." *International Journal of Remote Sensing* (accepted on Oct. 14, 2014).

Lu, J., L. Giustarini, B. Xiong, L. Zhao, Y. Jiang, Y. and B. Kuang. 2014. "Automated flood detection with improved robustness and efficiency using multi-temporal SAR data." *Remote Sensing Letters* 5(3): 240-248.

Ma, M. X. Wang, F, Veroustraete, and L. Dong. 2007. "Change in area of Ebinur Lake during the 1998–2005 period." *International Journal of Remote Sens*ing *28(24)*: 5523–5533.

Martinis, S. 2010. "Automatic near real-time flood detection inhigh resolution X-band synthetic aperture radar satellite data using context-based classification on irregular graphs." Ph.D. thesis. University of Munchen.
Martinis, S., A. Twele, and S. Voigt. 2009. "Towards operational near real-time flod detection using a split-based automatic thresholding procedure on high resolution TerraSAR-X data." *Natural Hazards and Earth System Sciences* 9: 303-314.
Molders, N. and A. Raabe. 1996. "Numerical investigations on the influence of subgrid-scale surface heterogeneity on evapotranspiration and cloud processes." *Journal of Applied Meteorology* 35(6): 782-795.
Ng, H. F. 2006. "Automatic thresholding for defect detection." *Pattern Recognition Letters* 27(14): 1644-1649.
Riordan, B., D. Verbyla, and A. D. McGuire. 2006. "Shrinking ponds in subarctic Alaska based on 1950-2001 remotely sensed images." *Journal of Geophysical Research* 111, G04002, doi:10.1029/2005JG000150.
Rundouist, D., S. Narumalani, and R. Narayanan. 2001. "A review of wetlands remote sensing and defining new considerations." *Remote Sensing Reviews* 20(3): 207–226.
Samanta, D., and M. Paul. 2011. "A novel approach of entropy based adaptive thresholding technique for video edge detection." *International Journal of Computer Science and Information Technologies* 2(5): 2108-2110.
Samanta, D., and G. Sanyal. 2012. "Classiciation of SAR images based on entropy." *International Journal of Computer Science and Information Technologies* 4(12): 82-86.
Schumann, G., R. Hostache, , C. Puech, L. Hoffmann, P. Matgen, F. Pappenberger, and L. Pfister. 2007. "High-resolution 3-D flood information from radar imagery for flood hazard management." *IEEE Transactions on Geoscience and Remote Sensing* 45(6): 1715–1725.
Sheng, Y., P. Gong, P., and Q. Xiao. 2001. "Quantitative dynamic flood monitoring with NOAA AVHRR." *International Journal of Remote Sensing 22(9)*: 1709–1724.
Shu, Y., J. Li, and G. Gomes. 2010. "Shoreline extraction from Radarsat-2 intensity imagery using a narrow band level set segmentation approach." *Marine Geodesy* 33(2): 187-203.
Smith,J.B., S. Agrawala, P. Larsen, and F.Gagnon-Lebrun. 2005. "Climate analysis. Bridge Over Troubled Waters Linking Climate Change and Development." S.Agrawala, Ed., OECD, Paris, 45-59.
Solbo, S., E. Malnes, T. Guneriussen, I. Solheim, and T. Eltoft. 2003. "Mapping surface-water with Radarsat at arbitrary incidence angles." *IGARSS '03 Proceedings* 4: 2517-2519.
Song, Y., H. Sohn, and C. Park. 2007. "Efficient water area classification using Radarsat-1 SAR imagery in a high relief mountainous environment." Photogrammetric Engineering & Remote Sensing 73(3): 285-296.
Sophocleous, M. 2002. "Interactions between groundwater and surface water: the state of the science." *Hydrogeology Journal* 10: 52–67.
Tulbure, M., and M. Broich. 2013. "Spatiotemporal dynamic of surface water bodies using Landsat time-series data from 1999 to 2011." *ISPRS Journal of Photogrammetry and Remote Sensing* 79(5): 44-52.
Yoshikawa , K. and L.D. Hinzman. 2003. "Shrinking thermokarst ponds and groundwater dynamics in discontinuous permafrost near Council, Alaska." *Permafrost Periglacial. Process* 14(2): 151-160. DOI:10.1002/ppp.451.
Wang, S., J. Huang, J. Li, A. Rivera, D.W. McKenney, and J. Sheffield. 2014a. "Assessment of water budget for sixteen large drainage basins in Canada." *Journal of Hydrology* 512: 1-15. doi: 10.1016/j.jhydrol.2014.02.058.
Wang, S, D.W. McKenney, J. Shang, and J. Li. 2014b. "A national-scale assessment of long-term water budget closures for Canada's watersheds." *Journal of Geophysical Research.* 119: 8712–8725. doi: 10.1002/2014JD021951.

Wang, S., J. Huang, D. Yang, G. Pavlic, and J. Li. 2014c, "Long-term water budget imbalances and error sources for cold region drainage basins." *Hydrological Processes* (accepted), doi: 10.1002/hyp.10343.
Wang, S., Y. Yang, and A. Rivera. 2013. "Spatial and seasonal variations in actual evapotranspiration over Canada's landmass." *Hydrology Earth System Sci.* 17: 3561–3575. doi:10.5194/hess-17-3561-2013.
Wang, S., A. P. Trishchenko, K. V. Khlopenkov, and A. Davidson. 2006. "Comparison of International Panel on Climate Change Fourth Assessment Report climate model simulations of surface albedo with satellite products over northern latitudes." *Journal of Geophysical Research.* 111, D21108, doi:10.1029/2005JD006728.